Hierarchical Gold-Decorated Magnetic Nanoparticle Clusters with Controlled Size

Carla J. Meledandri,[†,§] Jacek K. Stolarczyk,[†,^] and Dermot F. Brougham[†,‡,*]

[†]School of Chemical Sciences, Dublin City University, Glasnevin, Dublin 9, Ireland and [‡]National Institute for Cellular Biotechnology, Dublin City University, Glasnevin, Dublin 9, Ireland. [§] Present address: Department of Chemistry, University of Otago, Dunedin 9054, New Zealand. [^] Present address: Department of Physics, Ludwig-Maximilians-University Munich, Amalienstrasse 54, 80799 Munich, Germany.

ABSTRACT We present a new route to stable magnetic-plasmonic nanocomposite materials with exceptional control over composite size and very high monodispersity. The method involves the assembly of magnetic iron oxide nanoparticles, of any size in the superparamagnetic size range, whose steric repulsion is gradually reduced by competitive stabilizer desorption arising from the presence of a tertiary silica phase. Subsequent addition of gold nanoparticles results in hierarchical assemblies in the form of gold-decorated magnetic nanoparticle clusters, in a range of possible sizes from 20 to 150 nm, selected by the timing of the addition. This approach adds plasmonic and chemical functionality to the magnetic clusters and improves the physical robustness and processability of the suspensions. Most critically, detailed NMR relaxation analysis demonstrates that the effect of the gold NPs on the interaction between bulk solvent and the magnetic moments of the cluster is minimal and that the clusters remain superparamagnetic in nature. These advantages enhance the potential of the materials as size-selected contrast agents for magnetic resonance imaging. The possibility of generalizing the approach for the production of hierarchical assemblies of variable composition is also demonstrated.

KEYWORDS: magnetic nanoparticles · hybrid nanostructures · size control · magnetic resonance imaging

Stable suspensions of magnetic nanoparticles (NPs) have great potential for biomedical applications, notably for improved medical diagnosis[1−3] and targeted drug delivery.[4] In current applications as magnetic resonance imaging (MRI) contrast agents, iron oxide NPs are used to produce strong magnetic resonance relaxation enhancements,[5−7] as the large magnetic moments of the particles enhance image contrast in tissues containing the agent. Iron oxide NPs have also been envisaged as drug delivery vehicles which can be localized at a site of interest through the application of external magnetic fields.[4] Assembly of individual magnetic NPs into larger nanoparticle clusters (NPCs) can provide a general route to materials with higher magnetization. Biomedical applications of iron oxide NPCs are particularly dependent on the ability to control cluster size, architecture, and surface composition, as these properties largely determine biodistribution and the extent of contrast enhancement.

The iron oxide phases magnetite (Fe_3O_4) and maghemite (γ-Fe_2O_3) have similar magnetic properties and have both been investigated for biomedical applications; for the purposes of this article we shall refer to these phases as FeO. Methods for producing size-controlled magnetic FeO NPCs usually involve the *in situ* formation and stabilization of the NPs in the presence of polymers. Prominent examples include the alkaline coprecipitation of iron salts in the presence of random copolymers of styrenesulfonic, vinylsulfonic acid and acrylic acid.[8] In these cases the size of the aggregates formed was found to be influenced by the fractional coating of the magnetite cores and the surface chemistry of the polymer. Therefore, for a given polymer, stable suspensions could only be produced within a narrow size range, and larger clusters were associated with low NP loading. The difficulty in producing stable clusters arises from the fact that the nanoparticles must be unstable themselves for clustering to occur (solvophobic conditions), hence the resulting clusters are only marginally stable. Another promising approach is the single-step high temperature hydrolysis approach using poly(acrylic acid) as the surfactant in the solvent diethylene glycol.[9] In this case, the concentration of the base used in the reaction was shown to provide control over the NPC size; however, the primary NP size was 9−10 nm and could not be controlled.

We recently reported an alternative method for producing stable suspensions of NPCs with high NP loading and very tight control over NPC size.[10] Stable heptane suspensions of

* Address correspondence to dermot.brougham@dcu.ie.

Received for review September 8, 2010 and accepted January 19, 2011.

Published online February 10, 2011
10.1021/nn102331c

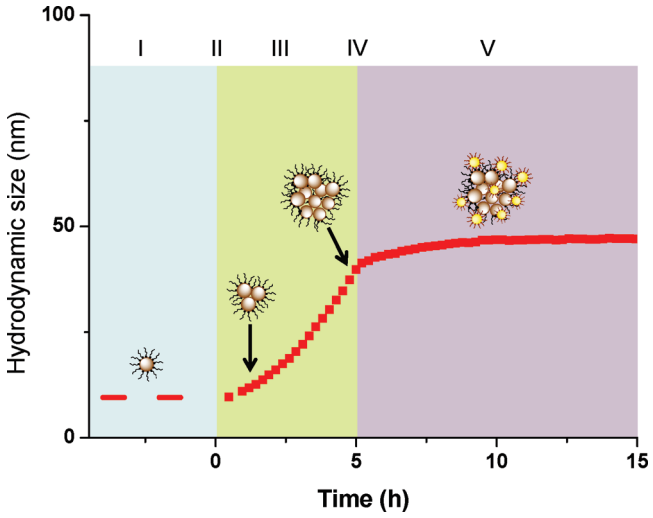

Scheme 1. Flow diagram for the process: (I) provide a suspension of iron oxide NPs of the first type (select particle size and phase); (II) initiate assembly by placing the suspension over the substrate; (III) continuously monitor cluster assembly; (IV) when the desired cluster size has been achieved, terminate assembly by adding NPs of a second type (*e.g.*, Au NPs) to produce stable functionalized hierarchical clusters.

monodisperse, fatty acid-stabilized Fe_3O_4 NPCs with sizes ranging from 50 to 200 nm were produced through competitive stabilizer desorption. The unique feature of this approach is that previously stable NP suspensions are perturbed by the introduction of a tertiary phase that competes for the stabilizer. Under appropriate conditions this intervention produces continuous and ongoing assembly of monodisperse NPCs over a period of hours. Effectively, an instability of external origin is introduced to the suspension which drives cluster formation by gradual reduction of steric repulsion between NPs. The advantage lies in the temporal nature of the controlled assembly, which allows external interventions, including the removal of the instability, to be made at a time of choice. A further unique advantage of our approach, which is demonstrated here for the first time, is that since the initial NP suspensions are stable (solvophilic conditions), the size of the primary NPs can be selected by any of a number of methods.[11] This provides a further aspect of control, as the magnetic properties of NPs, and the resulting NPCs, are very strongly dependent on NP size.[11−13]

In addition to good control over size, the next generation of nanoscale devices for biomedical applications will incorporate multiple functionalities. An established method to improve functionality of iron oxide nanoparticles is to incorporate noble metals, particularly gold, producing FeO/Au hybrid plasmonic−magnetic nanocomposites.[14−16] The most common architecture involves coating FeO cores with a complete layer, or shell, of gold, producing FeO@Au core@shell nanoparticles. The gold shell imparts many favorable properties on the magnetic cores.[17−20] This is largely due to plasmon resonance effects, but also arises from the well-established surface chemistry of the gold which facilitates conjugation of hydrophilic ligands and bioactive molecules. Control of the thickness of the Au shell remains a challenge, however. The presence of a complete layer of gold around iron oxide NPs may reduce the saturation magnetization, M_s. Values of 66 and 15 emu·g^{-1} were reported for nanoparticulate Fe_3O_4 and Fe_3O_4@Au, respectively,[21] reducing the usefulness of this type of material for MRI applications. The preparation of Au NPs conjugated to FeO NPs has also been reported. Negatively charged, 2−3 nm Au NPs were chemically attached onto amino-siloxane (APTES)-coated ~10 nm Fe_3O_4 nanoparticles,[22] producing stable ethanol suspensions. The addition of Au NPs had minimal effect on M_s; a 7% reduction was reported, and so this may be a more appropriate architecture for functionalized magnetic iron oxide nanostructures. However, to extend the use of these materials to applications such as T_2 contrast agents, or as drug delivery vehicles, new strategies are required to produce clusters of a desired size with tailored Au composition.

Herein we report the preparation of hybrid nanoparticle clusters of iron oxide (either γ-Fe_2O_3 or Fe_3O_4) NP decorated, or coated, with diamagnetic Au NPs. To our knowledge, this is the first report of the preparation of such materials in which the size of the composite is fully under experimenter control throughout the cluster assembly process. Importantly, the three steps of the preparation, that is, synthesis of NPs, cluster assembly, and surface decoration, are separate and so NP and NPC size and composition can all be controlled independently. These advantages of the process are illustrated in Scheme 1. We also show that the method can be applied to decoration of iron oxide NPCs with other types of nanoparticles, such as magnetic cobalt ferrite. These advantages permit the same process to be used to prepare a wide range of hierarchical

materials of selectable size, composition, and properties. The effect of added Au NP functionality on the critical physical properties of stable iron oxide suspensions was studied by dynamic light scattering (DLS), NMR, and transmission electron microscopy (STEM and TEM).

RESULTS AND DISCUSSION

Preparation and Primary Characterization of Size-Controlled FeO−Au NPC Suspensions. Monodisperse primary γ-Fe_2O_3 NP suspensions in heptane, of hydrodynamic size *ca.* 8 nm, were prepared using methods previously reported,[11] which are derived from the process described by Sun and Zeng.[23] The NPs were stabilized in suspension by a monolayer of mixed oleic acid/oleylamine surfactant molecules. Suspensions of *ca.* 15 nm monodisperse primary Fe_3O_4 NPs coated with oleic acid were prepared as described previously.[10] In a typical NPC assembly experiment 1.2 mL of a heptane NP suspension (of either type), containing 1−8 mM of Fe, was placed in a standard cuvette over 50.0 mg of cyanopropyl-modified 50 ± 20 μm silica particles (silica-CN, Alltech Associates), which formed a thin layer at the bottom. The controlled assembly of monodisperse NPCs by gradual aggregation of NPs was then observed by continuously monitoring the suspensions using DLS. A gradual increase in the *z*-, or number-, average hydrodynamic size was observed over several hours. There was, however, little change in the polydispersity index (PDI), which remained *ca.* 0.20, even after the addition of the second type of NP. The *z*-average and PDI are derived from cumulants analysis of the correlation function for the temporal fluctuations of the backscattered light intensity. PDI values of less than 0.25 are consistent with a monodisperse suspension, in which case the *z*-average can be used as a measure of the hydrodynamic size, d_{hyd}.

Subsequent addition of 50 μL of a heptane suspension of dodecanethiol (DDT)-stabilized Au NPs[24] (d_{hyd} = 7.7 nm, [Au] = 0.03 mM) to the suspensions of FeO NPCs, at different times during cluster assembly resulted in drastic attenuation of further cluster growth in all cases, irrespective of the rate of growth or the cluster size at the time of addition. This approach was used to prepare stable suspensions of γ-Fe_2O_3−Au NPCs of four different sizes, as shown in Figure 1. The ratio of initial Fe concentration to Au concentration corresponds to a mole ratio of approximately 33:1. Previous results[10] demonstrate that upon growing FeO NPCs to a d_{hyd} of 200 nm, at least 60% of the original Fe content remains in suspension. Hence, in all the experiments presented here, the FeO NPs were in a very large excess at the time of the Au NP addition. There is some variation in the rate of assembly during this stage. We have found the kinetics to be sensitive to the starting conditions; this will be the subject of a forthcoming manuscript. In the early stages of the

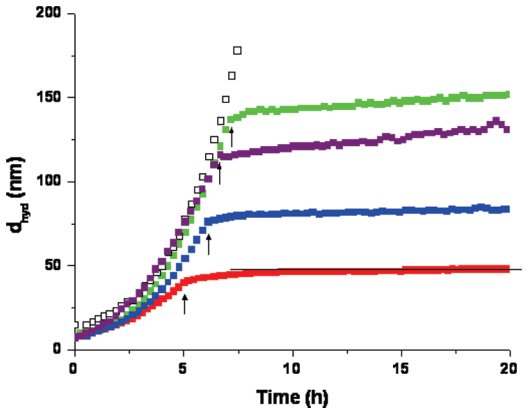

Figure 1. Light scattering data for a series of magnetic NPCs suspensions formed from γ-Fe_2O_3 NPs, assembled under similar conditions over CN-modified silica (50.0 mg). The initial NP suspensions had d_{hyd} = 8 nm, PDI = 0.15−0.20. The PDI values remained low over the course of the experiments. Assembly was stopped at the times indicated with arrows by the addition of Au NPs in suspension, but was allowed to proceed without addition for one sample (open marks). A horizontal line is superimposed over the 48 nm NPCs (red squares).

experiment (≤5 h), corresponding to smaller NPCs, assembly could be stopped completely with this concentration of Au NPs. When the Au NP addition took place at a later stage in the process (>6.5 h), assembly was significantly attenuated, but not stopped completely. The NPCs in suspensions to which no Au NP addition was made were observed to continue to increase in size. Very similar effects could be produced (Supporting Information) on adding Au NPs to Fe_3O_4 NPCs during assembly.

To confirm that gold-decorated clusters have been produced, several minutes after the addition of Au-NPs to growing Fe_3O_4 NPCs a drop of the suspension was removed from the cuvette, diluted as necessary, and air-dried onto a carbon-coated copper TEM grid. TEM micrographs from a Fe_3O_4−Au suspension with d_{hyd} = 112 nm are shown in Figure 2; additional images are provided in the Supporting Information. The TEM images show that the clusters have a three-dimensional appearance and Au NPs can be discerned on the clusters, due to their strong contrast. STEM images (Figure 2b) confirm that well-defined clusters are the dominant feature across the grids. There is no indication from the microscopic analysis of dendritic, or fractal, structure. Hence NPC assembly is reaction- as opposed to diffusion-limited.[25] The clusters are compact and dense when dry but are not particularly spherical. This is as expected given that under the solvophilic conditions used there is no driving force for the reduction of the surface area of the cluster. A more spherical shape is likely to be adopted upon subsequent phase transfer to solvophobic (*e.g.*, aqueous) environment. At the low Au concentrations used in this study very few dispersed Au NPs were observed in the images, demonstrating that the majority of the Au NPs

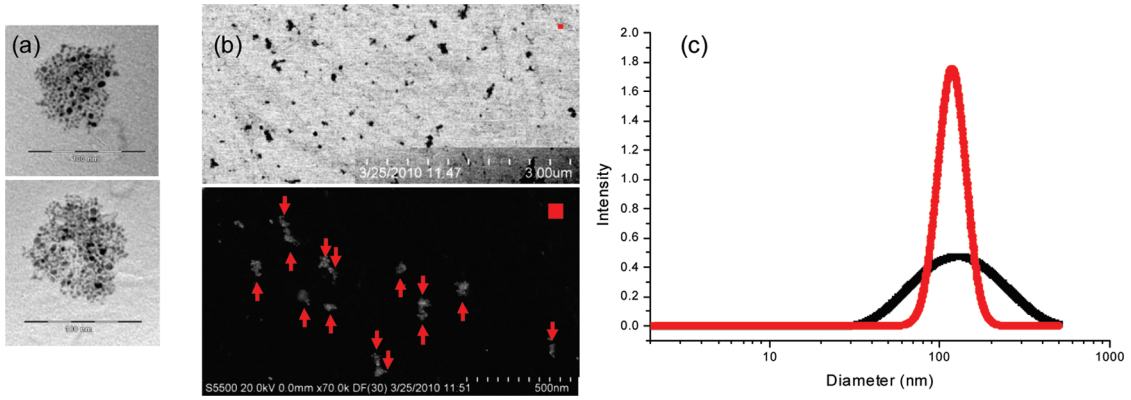

Figure 2. (a) TEM images of typical clusters from a Fe_3O_4−Au NPC suspension removed from silica when d_{hyd} = 112 nm, the scale bars are 100 nm, Au NPs appear as darker spots. (b) Representative STEM images of a Fe_3O_4−Au NPC sample with d_{hyd} = 112 nm, d_{STEM} = 71 nm; upper image low resolution bright-field STEM; lower image dark-field STEM with clusters indicated. In the upper right-hand corner of each STEM image a red square of side equivalent to 71 nm is provided as a guide. (c) Overlay of scattering intensity distributions for the sample presented in panel b; the experimental DLS distribution (black) and the simulated (Mie theory) distribution corresponding to the STEM size distribution (red).

adsorb onto the NPCs in suspension, and are retained during the drying process.

Statistical analysis of cluster size was conducted by measuring all the features in 18 separate STEM images from two separate grids. Multiple images were needed as dilution was required to prevent substantial overlap of clusters, on drying. The analysis resulted in an average cluster size of 71.5 nm with a SD of 13.5 nm (111 clusters). The size distribution is narrow, while the average size is somewhat lower than the hydrodynamic size of 112 nm obtained from cumulants analysis. However, comparison of the experimental light scattering intensity distribution (from DLS) and the simulated scattering intensity distribution generated using Mie theory[26,27] from the STEM size distribution shows excellent agreement (Figure 2c). This demonstrates that the two techniques measure the same size distribution and we can conclude that STEM analysis confirms the production of Au NP-decorated Fe_3O_4−Au NPCs of selected and controlled size. The DLS distribution is broad in comparison to that obtained from STEM, due to the high sensitivity of the DLS technique to outliers of the distribution (in particular to a very small number of larger aggregates).[11] The advantages of DLS measurements, however, lie in their potential to continuously monitor the entire population and to sensitively detect any *changes* in the width of the distribution.

TEM and STEM images were also obtained for γ-Fe_2O_3−Au NPCs following the attenuation of their assembly at d_{hyd} = 65 nm. The nanoparticulate material found on these grids was in the form of loose aggregates, with a flattened (or quasi-2D) appearance, with size significantly in excess of the DLS size. It is clear therefore, that Au-decorated clusters of both γ-Fe_2O_3 and Fe_3O_4 NPs can be prepared using competitive stabilizer desorption, but the properties of the two types of clusters are different. We anticipate that the major difference arises due to the strength of the magnetic moment per particle, which is far lower for γ-Fe_2O_3. This is primarily because the nanoparticles formed using thermal decomposition are of significantly smaller size, irrespective of the iron oxide phase present.

To further investigate the mechanism of cluster assembly, an experiment using γ-Fe_2O_3 NPs was carried out with three points of intervention, and the effect on d_{hyd}, PDI, and the backscattered light intensity was investigated (Figure 3). Upon addition of the Au NP suspension, NPC assembly was found to be significantly attenuated, and a decrease in the scattered light intensity was observed due to a slight change in the refractive index of the medium. Subsequent removal of the NPC suspensions from over the silica immediately stopped further assembly, and we observed no further change in scattered light intensity after the removal, confirming that there was no significant decrease in the concentration of the suspended NPCs in the absence of silica-CN. Upon re-exposure of the suspension to fresh silica, cluster assembly was found to resume. This suggests that our approach has potential for the preparation of size-controlled nanostructures with radially variable or multilayered composition.

The results presented in Figure 3 demonstrate that silica is an ongoing requirement for cluster assembly. We also found that adding free DDT, in the 1−47 mM range had no effect on the rate of assembly of γ-Fe_2O_3 NPCs, confirming that intact DDT-stabilized Au NPs, as opposed to free thiol molecules, are responsible for the attenuation. This observation is expected, considering the strength of the Au−S bond[28] meaning that the Au NPs do not act as a source of free DDT. It should also be noted that no evidence of cluster formation, or Au NP loss, was detected for a pure suspension of DDT-stabilized Au NPs (d_{hyd} = 7.7 nm, [Au] = 0.71 mM) placed over silica for 20 h. These observations indicate that the attenuation is not caused by blockage of the

adsorption sites on the silica substrate by Au NPs. The microscopic investigations confirm that the Au NPs directly interact with FeO NPCs and limit further increase in cluster size.

Hence by continuously monitoring the NPC assembly process using DLS, we have shown that both γ-Fe_2O_3 (Figure 1) and Fe_3O_4 NPs (Supporting Information) can be used to produce suspensions of FeO−Au NPCs of selected and, hence, reproducible size. The mechanism for cluster assembly has been described previously.[10] Essentially the silica provides a sink for free surfactant molecules in suspension, which alters the equilibrium between NP-bound and free surfactant. This generates a very low concentration of nanoparticles which are partially depleted of surface-bound surfactant molecules, that is, with vacant, non-coated sites on their surfaces, thereby reducing their steric repulsion. We have previously shown that assembly of Fe_3O_4 NPCs can be arrested at any time by addition of oleic acid (*i.e.*, excess surfactant) which eliminates these vacant sites. The results presented here demonstrate that DDT-stabilized Au NPs can have a similar effect, allowing us to produce, for the first time, stable suspensions of binary, functionalized magnetic nanocomposite materials of complex composition, with controlled size over a wide size range (40−150 nm), Scheme 2.

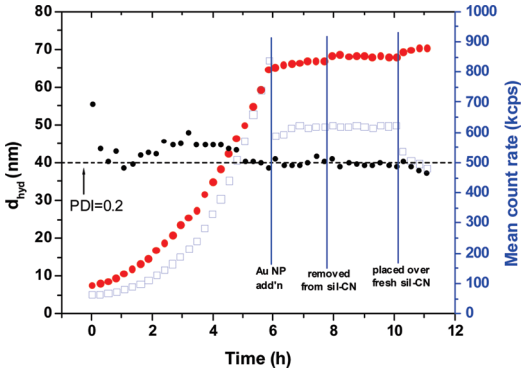

Figure 3. Typical DLS data for assembly of γ-Fe_2O_3 NPs observed by DLS; d_{hyd} (red) and corresponding backscattered light intensity (blue) for a sample placed over CN-modified silica (50.1 mg). The PDI values (black) are shown to improve slightly over the course of the experiment. Further cluster assembly was stopped when the d_{hyd} value reached 65 nm by the addition of Au NPs in suspension.

We propose that the Au NPs physisorb onto the less perfect oleate-coated surface of the FeO NPCs (*i.e.*, "vacant sites"), perhaps filling spaces between particles on the NPC surface (Scheme 2). The micrographs shown in Figure 2 clearly show that the adsorbed Au NPs have no affinity for each other and hence are dispersed across the surface of the clusters. Hence, we show here that the vacant sites rather than being the source of instability of the NPCs, constitute ideal places for their functionalization with nanoparticles of a different type. On the other hand, further addition of FeO NPs results in ongoing cluster assembly, as these NPs are subject to competitive stabilizer desorption.

Magnetic Resonance Properties of Size-Controlled γ-Fe_2O_3−Au NPC Suspensions. The magnetic γ-Fe_2O_3−Au nanocomposites, removed from over the silica−CN, were characterized in suspension by field-cycling NMR relaxometry.[10,11,29] In this technique the spin-lattice relaxation enhancement per mM of Fe (the relaxivity r_1) is recorded as a function of ^{1}H Larmor frequency. The values of r_1 can be determined according to Equation 1, with knowledge of the solvent relaxation time, and the Fe concentration (in mM).

$$r_1 = \frac{R_{1,\,obs} - R_{1,\,solv}}{[Fe]} \qquad (1)$$

Where $R_{1,obs}$ (= $1/T_{1,obs}$) is the measured spin−lattice relaxation rate at a given frequency, $R_{1,solv}$ is the rate in the absence of any enhancement, and the relaxivity, r_1, has units of s^{-1} mM^{-1} . The influence of the magnetic properties of the suspended particles on the shape of the profile can be interpreted on the basis of the work of the Muller group.[12,30] Hence NMR profiles have been used to characterize the magnetic

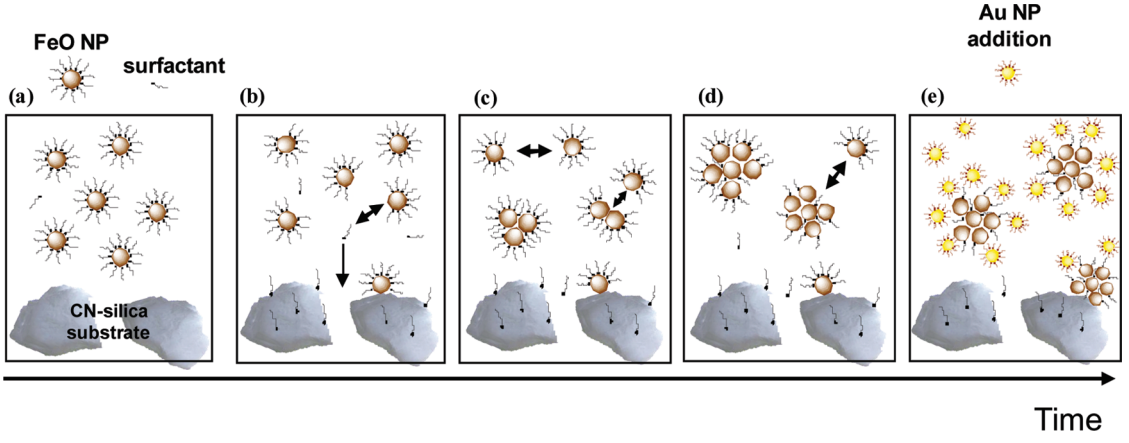

Scheme 2. Schematic representation of the process: (a,b) activation of iron oxide NPs through action of silica; (c,d) formation of clusters by addition of NPs to NPs and subsequently to clusters; (e) addition of Au NPs which interact with the NPC surface.

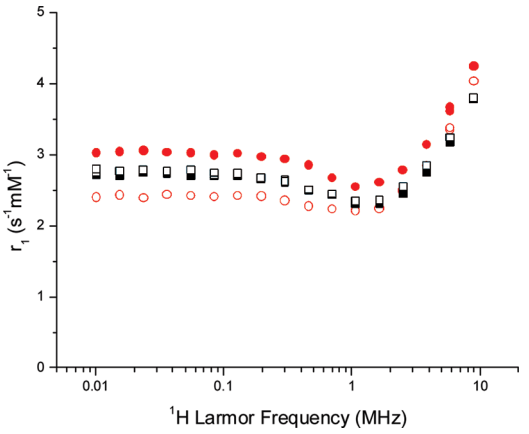

Figure 4. ^{1}H relaxation profiles, recorded at 298 K in heptane, for suspensions of (i) γ-Fe_2O_3 NPCs, fresh suspension (red filled circles) d_{hyd} = 93 nm, [Fe] = 1.51 mM, and after resuspension (red open circles) d_{hyd} = 103 nm, [Fe] = 1.13 mM, equivalent to 75% of the material being resuspended; (ii) γ-Fe_2O_3−Au NPCs, fresh suspension (black filled squares) d_{hyd} = 88 nm, [Fe] = 1.41 mM, and after resuspension (black open squares) d_{hyd} = 86 nm, [Fe] = 1.30 mM, equivalent to 92% of the material being resuspended.

properties of aqueous[12,31,32] and nonaqueous suspensions,[10,11] providing quantitative measures of NP size and M_s.[11] However, unlike magnetometry, relaxometry is particularly sensitive to the interaction of the solvent molecules with the moments of the NPs at the surface of the clusters. It is these specific interactions, as opposed to the bulk magnetic properties, that determine r_1 and hence the utility for MRI applications.

In Figure 4 the NMR profiles for γ-Fe_2O_3 and γ-Fe_2O_3−Au NPCs of similar size are presented. These suspensions were removed from over silica with average hydrodynamic sizes of 93 and 88 nm, respectively. Errors in r_1 are always less than 1% and the experiments are highly reproducible, indicating the stability of the suspensions and robustness of the technique. The profile for γ-Fe_2O_3 NPCs (Figure 4, red filled circles) exhibits all the features of superparamagnetic ^{1}H relaxation and is almost identical to that of dispersed primary NPs.[11] In particular the presence of the mid-frequency r_1 minimum demonstrates the presence of very weak interparticle interactions within the clusters, due to the presence of residual surfactant (ligand) molecules. This feature is normally only observed for physically dispersed superparamagnetic NPs of small size,[30] but not for nanoparticle clusters.[32] It arises because at low frequency the particle moments are no longer locked to the external field, and the ^{1}H relaxation is driven by the Néel process (reorientation of the magnetic moments in the local magnetocrystalline field). In the case of increased magnetocrystalline anisotropy, arising from larger nanoparticle size, or from greater inherent anisotropy of the nanoparticles, or due to interparticle interactions, this contribution to the relaxation becomes non-dispersive in the mid-frequency range, and the minimum is not observed.[30] The nature of this effect has been confirmed experimentally; a minimum was observed in the case of small iron oxide nanoparticles doped with a very low fraction of cobalt, but it was suppressed on increasing the cobalt content.[33] Cobalt is known to increase the magnetocrystalline anisotropy.

The profile of γ-Fe_2O_3−Au NPCs (Figure 4, black filled squares) of approximately the same size has almost identical shape, with systematically lower relaxivity values across the frequency range. In fact, scaling this curve up by a factor of 1.12 gives perfect agreement at all frequencies with the profile of γ-Fe_2O_3 NPCs, see Supporting Information. This clearly demonstrates that the relaxation rate per mM of Fe is slightly reduced due to diamagnetic shielding by the partial Au NP coating despite the fact that the Au NP layer is not complete. This decrease is close to the 7% reduction in M_s, reported for FeO−Au nanocomposites with the same architecture.[22] Although in that case Au NPs were bound to predominantly dispersed, that is, individual, FeO NPs. It should be emphasized that, aside from scaling the relaxivity, the profiles are not changed by the addition of Au NPs; the mid-frequency minimum and low frequency plateau are not affected. Hence the effective magnetocrystalline anisotropy of the iron oxide NPs, arising from dipolar interparticle interactions within the clusters, does not change. This is further confirmation that the addition of Au NPs is a surface effect.

Physical Properties of Size-Controlled γ-Fe_2O_3−Au NPC Suspensions. After recording the NMR profiles, both suspensions were dried in a cuvette under a steady stream of N_2. Upon drying, the same volume (1.2 mL) of heptane was added to resuspend each sample; the samples were shaken by hand, allowed to stand for 30 min, shaken again, and reanalyzed by DLS and NMR. For resuspended γ-Fe_2O_3−Au NPCs 92% (by Fe determination) of the material was resuspended and the original NMR profile was recovered (Figure 4, black squares) demonstrating that the magnetic resonance properties were unaffected, the d_{hyd} and PDI values also showed no measurable change. The reconstituted suspension was found to be stable for many days. This is an interesting result, particularly when one considers that the clusters did not produce good STEM images, although in that case drying was onto a carbon-coated grid, as opposed to a glass surface.

On the other hand for unmodified γ-Fe_2O_3 NPCs a significant change in size, from 93 to 103 nm, was observed on resuspension. Less material, approximately 75% of the original, was recovered after drying, while the altered shape of the ^{1}H NMR relaxation profile (Figure 4, red circles) demonstrates a change in the organization of the NPs within the resuspended clusters. In particular, the loss of the mid-frequency minimum can only arise from increased magnetocrystalline anisotropy energy due to stronger interparticle interactions in the clusters.[30] Size control is clearly lost

during drying and resuspension of the non-functionalized clusters, and the redistributed iron oxide particles in the clusters have markedly different magnetic properties and are far less stable over time. In fact this suspension was far less stable than the original γ-Fe_2O_3 NPC suspension; the d_{hyd} continued to increase (to 400−800 nm), as did the PDI, and the suspension precipitated completely over a few days. Multiple attempts were made to reproduce the behavior observed for γ-Fe_2O_3−Au NPC suspensions, but invariably the unmodified clusters could not be resuspended unchanged.

Improved physical stability of FeO−Au NPC suspensions is also apparent from the following: (i) Extended lifetimes of the nanocomposite suspensions; the NMR and DLS responses of freshly prepared FeO−Au NPC suspensions are stable for weeks (as opposed to days for FeO NPCs). (ii) Improved thermal stability; the FeO−Au NPC suspensions can be heated to 60 °C for 40− 60 min, and the NMR and DLS responses are fully recovered upon returning to room temperature. (iii) Stability to dilution into the sub-millimolar range (Fe concentration). None of these effects can be achieved for nonfunctionalized NPCs, see Supporting Information.

Thus Au NPs are found to significantly improve the physical characteristics of the suspensions, without significantly altering their favorable relaxivity. Hence Au-NP decoration is an optimal architecture for maintaining high relaxivity and retaining the favorable superparamagnetic properties of the suspensions. Furthermore, the inclusion of Au NPs may provide new opportunities for the integration of multiple functions onto the magnetic carrier. For instance, the optical properties of gold, combined with the magnetic properties of the core, may facilitate the use of the FeO−Au clusters for combined optical detection and magnetic resonance imaging. The Au NPs may also be used for adding further molecular functionalities.

General Applicability of the Methods. First, considering the formation of the iron oxide NPCs, it should be noted that our previous observations of NPC assembly were for Fe_3O_4 NPs formed by aqueous coprecipitation methods.[10] In the current work we also present observations of controlled cluster assembly for γ-Fe_2O_3 NPs prepared by thermal decomposition methods,[11] which are of smaller size and which are surface stabilized by both oleic acid and oleylamine.[34] This suggests that our approach for assembling clusters through competitive stabilizer desorption may be generally applicable. We also demonstrate that both types of clusters can be surface-functionalized with Au NPs.

Second, the possibility of using NPs of alternative composition, other than gold, to stabilize NPCs was investigated. Figure 5 shows attenuation of the assembly of NPCs, composed initially of Fe_3O_4 NPs, by the addition of oleic acid/oleylamine stabilized cobalt ferrite nanoparticles,[35] which are known to possess very high magnetocrystalline anisotropy.[33]

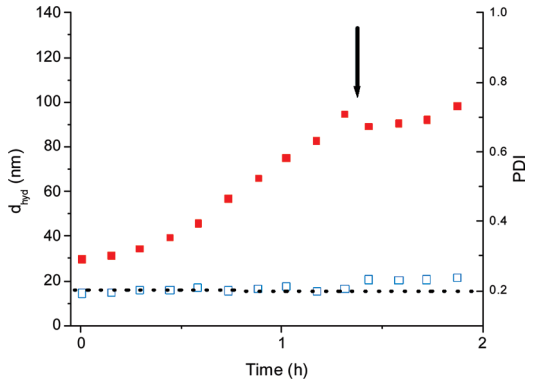

Figure 5. DLS data for Fe_3O_4 NPC assembly over CN-modified silica stopped by addition of a suspension of $CoFe_2O_4$ NPs. The time of addition is indicated with an arrow.

We are currently studying the effect of the extent of cluster coverage with ferromagnetic, and highly anisotropic, $CoFe_2O_4$ NPs (as opposed to diamagnetic Au NPs) on the magnetic resonance properties of the nanocomposite suspensions. One might also expect that in principle other types of metal, metal-oxide, metal-chalcogenide, or polymer nanoparticles could be used to attenuate NPC assembly, once these NPs are stabilized in nonaqueous media by extended alkyl chains. Hence the results presented here establish the possibility of using our approach to produce hierarchical-magnetic (-plasmonic or -fluorescent) assemblies of complex composition.

It should be noted that development of size-controlled magnetic NPCs for biomedical application requires colloidal stability in physiological media. The preparation of NPs using thermal decomposition methods,[23] in particular, remains an attractive choice due to the excellent control over NP size and morphology that it provides. Biomedical application of suspension of NPs, or of size-controlled NPCs, will require surface functionalization and phase transfer into water. Recent developments in this area[13,36] suggest many possible approaches, which we are currently pursuing, to accomplish this task; the improved physical robustness of FeO−Au NPCs will assist in this process. An alternative is to develop competitive stabilizer desorption in water.

CONCLUSIONS

We have presented a method for the assembly of size-selectable iron oxide nanoparticle clusters, in the size range up to 150 nm, which are surface functionalized with nanoparticles of a different composition. The nanocomposites have improved stability and consist of quasi-spherical clusters. Uniquely, our approach allows (i) the size of the primary nanoparticles (ii) the size of the nanoparticle clusters, and (iii) the composition of the functionalizing nanoparticles all to be adjusted independently. These innovations allow us

to tune the emergent magnetic resonance properties of the resulting stable nanocomposite suspensions, a significant advantage for applications in chemistry, biology, and medicine.

MATERIALS AND METHODS

Synthesis. All chemicals were purchased from Sigma Aldrich and used as received. Stable heptane suspensions of primary maghemite NPs were prepared using methods previously reported,[11] derived from the process described by Sun and Zeng.[23] Iron(III) acetylacetonate (2 mmol), 1,2-hexadecanediol (10 mmol), oleic acid (4.5 mmol), oleylamine (4.5 mmol), and diphenyl ether (20 mL) were combined and gradually heated to 265 °C to reflux for 15 min under a nitrogen atmosphere. The mixture was removed from the heat source and allowed to cool to room temperature. The NPs were precipitated by the addition of ethanol, and isolated by magnetic means. Following an additional washing step, the NPs were dispersed in 15 mL of *n*-heptane without addition of further surfactant. The suspension was centrifuged to remove any aggregates. The supernatant was retained for NPC assembly experiments and diluted as needed to 1.0−2.0 mM with heptane. Stable heptane suspensions of magnetite NPs were prepared by aqueous coprecipitation as described previously.[10]

Dodecanethiol-coated Au NPs were synthesized in a two-phase liquid−liquid system as described by Brust *et al.*[24] An aqueous solution of hydrogen tetrachloroaurate (10 mL, 30 mM) was added to a solution of TOAB in toluene (26.7 mL, 50 mM), and the mixture was vigorously stirred for 15 min. Dodecanethiol (67 μL) was added to the mixture. An aqueous solution of sodium borohydride (8.3 mL, 0.4 mM, freshly prepared) was added dropwise with vigorous stirring. The mixture was covered and stirred at room temperature for 3 h. The stirring was discontinued, and the organic phase was transferred to a separate flask. To precipitate the Au NPs from the organic phase, ethanol (~50 mL) was added, and the mixture was placed in a freezer (−20 °C, > 4 h). The precipitate was filtered under reduced pressure, washed with ethanol, and suspended in 40 mL of heptane. The suspension was centrifuged to remove any aggregates. The supernatant was retained for the assembly experiments and diluted as needed with heptane.

NMR Analysis. The ^{1}H relaxation profiles were measured over the frequency range 0.01−10 MHz using a Spinmaster FFC-2000 Fast Field Cycling NMR Relaxometer (Stelar SRL, Mede, Italy). The system operated at a measurement frequency of 9.25 MHz for ^{1}H. The sample temperature was controlled to 25 ± 0.2 °C using the Stelar VTC system. Full details of the methods are available elsewhere.[11,29] All of the ^{1}H magnetization recovery curves were monoexponential within error; the random errors in fitting T_1 were always less than 1%.

Quantitative Analysis. Samples were prepared for Fe determination using previously reported methods.[11] Total iron content was determined by either atomic absorption spectroscopy (AAS) on a Varian SpectrAA Spectrometer, using a Fe-cathode lamp light source with a wavelength of 248.3 nm, or by inductively coupled plasma atomic emission spectroscopy (ICP-AES) on a Varian Liberty 220ICP. All standard curves were highly linear; $R^2 > 0.995$ in all cases. The fitting error in R_1 is higher at 0.5−1.0%, so this is the largest source of errors in r_1. Error bars are included for r_1 in all figures, but are invariably smaller than the size of the data points.

Electron Microscopy. All TEM images were obtained using a JEOL 2000 FX TEMscan (at an accelerating voltage of 80 kV) for samples deposited on carbon-coated (400 mesh) copper grids. The preparation of samples for TEM analysis involved depositing a drop (15 μL) of the diluted relevant dispersion in heptane onto the grids and allowing the solvent to evaporate, prior to imaging. STEM images were obtained using a Hitachi S5500 Field Emission SEM (at an accelerating voltage of 20 kV) for samples deposited on carbon-coated (400 mesh) copper grids previously prepared for TEM analysis.

Acknowledgment. The authors would like to thank Dr. Brendan Twamley, DCU, for assistance with scanning electron microscopy. We also thank Sean Quilty (Particular Sciences) and Dr. Mike Kaszuba (Malvern) for input on the DLS measurements and Dr. David Cottell, University College Dublin, for access to TEM. We acknowledge support from Science Foundation Ireland (MASF666), including purchase of the FE-SEM, and Enterprise Ireland (POC/2006/207, CFTD/2008/135).

Supporting Information Available: Additional DLS data, additional micrographs, statistical analysis of micrographs, stability data for the suspensions, additional NMR analysis. This material is available free of charge *via* the Internet at http://pubs.acs.org.

REFERENCES AND NOTES

1. Xie, J.; Huang, J.; Li, X.; Sun, S.; Chen, X. Iron Oxide Nanoparticle Platform for Biomedical Applications. *Curr. Med. Chem.* **2009,** *16*, 1278–1294.
2. Lee, J.-H.; Huh, Y.-M.; Jun, Y.-W.; Seo, J.-W.; Jang, J.-T.; Song, H.-T.; Kim, S.; Cho, E.-J.; Yoon, H.-G.; Suh, J.-S.; Cheon, J. Artificially Engineered Magnetic Nanoparticles for Ultra-sensitive Molecular Imaging. *Nat. Med.* **2007,** *13*, 95–99.
3. Huh, Y.-M.; Jun, Y.; Song, H.-T.; Kim, S.; Choi, J.; Lee, J.-H.; Yoon, S.; Kim, K.-S.; Shin, J.-S.; Suh, J.-S.; *et al*. *In Vivo* Magnetic Resonance Detection of Cancer by Using Multifunctional Magnetic Nanocrystals. *J. Am. Chem. Soc.* **2005,** *127*, 12387–12391.
4. Barnett, B. P.; Arepally, A.; Karmarkar, P. V.; Qian, D.; Gilson, W. D.; Walczak, P.; Howland, V.; Lawler, L.; Lauzon, C.; Stuber, M.; *et al*. Magnetic Resonance-Guided, Real-Time Targeted Delivery and Imaging of Magnetocapsules Immunoprotecting Pancreatic Islet Cells. *Nat. Med.* **2007,** *13*, 986–991.
5. Bruns, O. T.; Ittrich, H.; Peldschus, K.; Kaul, M. G.; Tromsdorf, U. I.; Lauterwasser, J.; Nikolic, M. S.; Mollwitz, B.; Merkel, M.; Bigall, N. C.; *et al*. Real-Time Magnetic Resonance Imaging and Quantification of Lipoprotein Metabolism *In Vivo* Using Nanocrystals. *Nat. Nanotechnol.* **2009,** *4*, 193–201.
6. Na, H. B.; Lee, J. H.; An, K.; Park, Y. I.; Park, M.; Lee, I. S.; Nam, D.-H.; Kim, S. T.; Kim, S.-H.; Kim, S.-W.; *et al*. Development of a T_1 Contrast Agent for Magnetic Resonance Imaging Using MnO Nanoparticles. *Angew. Chem., Int. Ed.* **2007,** *46*, 5397–5401.
7. Park, J.-H.; von Maltzahn, G.; Zhang, L.; Schwartz, M. P.; Ruoslahti, E.; Bhatia, S. N.; Sailor, M. J. Magnetic Iron Oxide Nanoworms for Tumor Targeting and Imaging. *Adv. Mater.* **2008,** *20*, 1630–1635.
8. Ditsch, A.; Laibinis, P. E.; Wang, D. I. C.; Hatton, T. A. Controlled Clustering and Enhanced Stability of Polymer-Coated Magnetic Nanoparticles. *Langmuir* **2005,** *21*, 6006–6018.
9. Ge, J.; Hu, Y.; Biasini, M.; Beyermann, W. P.; Yin, Y. Superparamagnetic Magnetite Colloidal Nanocrystal Clusters. *Angew. Chem., Int. Ed.* **2007,** *46*, 4342–4345.
10. Stolarczyk, J. K.; Ghosh, S.; Brougham, D. F. Controlled Growth of Nanoparticle Clusters through Competitive Stabilizer Desorption. *Angew. Chem., Int. Ed.* **2009,** *48*, 175–178.
11. Meledandri, C. J.; Stolarczyk, J. K.; Ghosh, S.; Brougham, D. F. Nonaqueous Magnetic Nanoparticle Suspensions with Controlled Particle Size and Nuclear Magnetic Resonance Properties. *Langmuir* **2008,** *24*, 14159–14165.
12. Laurent, S.; Forge, D.; Port, M.; Roch, A.; Robic, C.; Vander Elst, L.; Muller, R. N. Magnetic Iron Oxide Nanoparticles: Synthesis, Stabilization, Vectorization, Physicochemical Characterizations, and Biological Applications. *Chem. Rev.* **2008,** *108*, 2064–2110.
13. Tromsdorf, U. I.; Bigall, N. C.; Kaul, M. G.; Bruns, O. T.; Nikolic, M. S.; Mollwitz, B.; Sperling, R. A.; Reimer, R.; Hohenberg, H.; Parak, W. J. Size and Surface Effects on the MRI Relaxivity

of Manganese Ferrite Nanoparticle Contrast Agents. *Nano Lett.* **2007,** *7*, 2422–2427.
14. Shevchenko, E. V.; Bodnarchuk, M. I.; Kovalenko, M. V.; Talapin, D. V.; Smith, R. K.; Aloni, S.; Heiss, W.; Alivisatos, A. P. Gold/Iron Oxide Core/Hollow-Shell Nanoparticles. *Adv. Mater.* **2008,** *20*, 4323–4329.
15. Larson, T. A.; Bankson, J.; Aaron, J.; Sokolov, K. Hybrid Plasmonic Magnetic Nanoparticles as Molecular Specific Agents for MRI/Optical Imaging and Photothermal Therapy of Cancer Cells. *Nanotechnology* **2007,** *18*, 325101.
16. Lim, J.; Eggeman, A.; Lanni, L.; Tilton, R. D.; Majetich, S. A. Synthesis and Single-Particle Optical Detection of Low-Polydispersity Plasmonic-Superparamagnetic Nanoparticles. *Adv. Mater.* **2008,** *20*, 1721–1726.
17. Lyon, J. L.; Fleming, D. A.; Stone, M. B.; Schiffer, P.; Williams, M. E. Synthesis of Fe Oxide Core/Au Shell Nanoparticles by Iterative Hydroxylamine Seeding. *Nano Lett.* **2004,** *4*, 719–723.
18. Kim, J.; Park, S.; Lee, J. E.; Jin, S. M.; Lee, J. H.; Lee, I. S.; Yang, I.; Kim, J.-S.; Kim, S. K.; Cho, M.-H.; *et al*. Designed Fabrication of Multifunctional Magnetic Gold Nanoshells and Their Application to Magnetic Resonance Imaging and Photothermal Therapy. *Angew. Chem., Int. Ed.* **2006,** *45*, 7754–7758.
19. Levin, C. S.; Hoffman, C.; Ali, T. A.; Kelly, A. T.; Morosan, E.; Nordlander, P.; Whitmire, K. H.; Halas, N. J. Magnetic-Plasmonic Core-Shell Nanoparticles. *ACS Nano* **2009,** *3*, 1379–1388.
20. Zhang, Q.; Ge, J.; Goebl, J.; Hu, Y.; Sun, Y.; Yin, Y. Tailored Synthesis of Superparamagnetic Gold Nanoshells with Tunable Optical Properties. *Adv. Mater.* **2010,** *22*, 1905–1909.
21. Wang, L.; Wang, L.; Luo, J.; Fan, Q.; Suzuki, M.; Suzuki, I. S.; Engelhard, M. H.; Lin, Y.; Kim, N.; Wang, J. Q.; Zhong, C.-J. Monodispersed Core-Shell Fe_3O_4@Au Nanoparticles. *J. Phys. Chem. B* **2005,** *109*, 21593–21601.
22. Caruntu, D.; Cushing, B. L.; Caruntu, G.; O'Connor, C. J. Attachment of Gold Nanograins onto Colloidal Magnetite Nanocrystals. *Chem. Mater.* **2005,** *17*, 3398–3402.
23. Sun, S.; Zeng, H. Size-Controlled Synthesis of Magnetite Nanoparticles. *J. Am. Chem. Soc.* **2002,** *124*, 8204–8205.
24. Brust, M.; Walker, M.; Bethell, D.; Schiffrin, D. J.; Whyman, R. Synthesis of Thiol-Derivatised Gold Nanoparticles in a Two-Phase Liquid−Liquid System. *Chem. Commun.* **1994,** *7*, 801–802.
25. Lin, M. Y.; Lindsay, H. M.; Weitz, D. A.; Ball, R. C.; Klein, R.; Meakin, P. Universality in Colloid Aggregation. *Nature* **1989,** *339*, 360–362.
26. Mätzler, C. *MATLAB Functions for Mie Scattering and Absorption*, 2ed.; University of Bern: Bern, Switzerland, 2002.
27. Bohren, C. F.; Huffman, D. R. *Absorption and Scattering of Light by Small Particles*; Wiley: Weinheim, Germany, 2004.
28. Ulman, A. Formation and Structure of Self-Assembled Monolayers. *Chem. Rev.* **1996,** *96*, 1533–1554.
29. Kimmich, R.; Anoardo, E. Field-cycling NMR relaxometry. *Prog. Nucl. Magn. Reson. Spectrosc.* **2004,** *44*, 257–320.
30. Roch, A.; Muller, R. N.; Gillis, P. Theory of Proton Relaxation Induced by Superparamagnetic Particles. *J. Chem. Phys.* **1999,** *110*, 5403–5411.
31. Byrne, S. J.; Corr, S. A.; Gun'ko, Y. K.; Kelly, J. M.; Brougham, D. F.; Ghosh, S. Magnetic Nanoparticle Assemblies on Denatured DNA Show Unusual Magnetic Relaxivity and Potential Applications for MRI. *Chem. Commun.* **2004,** *22*, 2560–2561.
32. Corr, S. A.; Gun'ko, Y. K.; Tekoriute, R.; Meledandri, C. J.; Brougham, D. F. Poly(sodium-4-styrene)sulfonate−Iron-Oxide Nanocomposite Dispersions with Controlled Magnetic Resonance Properties. *J. Phys. Chem. C* **2008,** *112*, 13324–13327.
33. Roch, A.; Gillis, P.; Ouakssim, A.; Muller, R. N. Proton Magnetic Relaxation in Superparamagnetic Aqueous Colloids: A New Tool for the Investigation of Ferrite Crystal Anisotropy. *J. Magn. Magn. Mater.* **1999,** *201*, 77–79.
34. Klokkenburg, M.; Hilhorst, J; Erné, B. H. Surface Analysis of Magnetite Nanoparticles in Cyclohexane Solutions of Oleic Acid and Oleylamine. *Vib. Spectrosc.* **2007,** *43*, 243–248.
35. De Palma, R.; Peeters, S.; Van Bael, M. J.; Van den Rul, H.; Bonroy, K.; Laureyn, W.; Mullens, J.; Borghs, G.; Maes, G. Silane Ligand Exchange to Make Hydrophobic Superparamagnetic Nanoparticles Water-Dispersible. *Chem. Mater.* **2007,** *19*, 1821–1831.
36. Zhang, T.; Ge, J.; Hu, Y.; Yin, Y. A General Approach for Transferring Hydrophobic Nanocrystals into Water. *Nano Lett.* **2007,** *7*, 3203–3207.